Article

Rare ice-base temperature measurements in Antarctica reveal a cold base in contrast with predictions

Check for updates

Pavel G. Talalay[1,2], German Leitchenkov[3,4], Vladimir Lipenkov[5], Youhong Sun[2,6], Nan Zhang ®[1] ✉,
Da Gong[1], Yunchen Liu[1], Yazhou Li[2], Yuchen Sun[2], Ilnur Abdrakhmanov[3], Mstislav Vorobyev[7],
Damir Khalimov[3], Xiaopeng Fan[8], Andrey Salamatin[5], Alexey A. Ekaykin ®[5] & Bing Li[2,6] ✉

The Antarctic bed demonstrates complex behaviour comprising alternating warm- and cold-based areas. However, the distribution of warm- and cold-based areas, basal melting rates, and the structure and age of the basal ice are not yet fully known. In the 2023–2024 season, we drilled an access borehole through 541 m thick ice at Princess Elizabeth Land, 28 km south of the coast. Temperature measurements at the bottom of the borehole revealed a cold underlying base despite a warm-based interface being predicted in advance as the most likely estimate. Our results imply that the Antarctic base can be locally colder than currently assumed, and that thermal models, especially basal boundary conditions, should be carefully specified and provided with the confirmed input data.

The Antarctic ice sheet is the largest reservoir of frozen freshwater in the world and one of the biggest contributors to sea-level rise[1]. The mass loss of the Antarctic ice sheet has more than tripled over the past three decades. The losses come from different sources: iceberg calving, ice shelf disintegration, surface ablation (if the meltwater runs off the ice sheet) and basal melt of the ice shelves and the continental warm-based areas. The input of the Antarctic ice sheet into the total sea-level rise over the 21st-century as predicted by the Sixth Assessment Report of the Intergovernmental Panel on Climate Change (IPCC) varies over a wide range, from 0.08 to 0.34 m, within the total global sea-level rise estimated at 0.40–1.01 m. The distribution by area and the rate of basal melting in the warm-based areas of the Antarctic ice sheet are among the most uncertain factors in the current sea-level projections, alongside ice-ocean interaction and surface mass balance sensitivity to the increasing air temperature[2–4].

A detailed study of ice-bed coupling is important not only in terms of projection of the sea level rise. It gives valuable insights to glaciologists, geologists, geomorphologists and paleoclimatologists. The basal thermal regime exerts a strong control on the ice sheet dynamics[5] and the ice age in the lower layers[6]. Any basal melting removes very old ice in the deepest parts of the ice sheet that represents a problem to the downward extension of the climate records[7]. The basal thermal conditions are primarily defined by geothermal heat flux supplied to the ice base from the Earth's interior coupled with the basal strain heating, as well as by ice thickness depending on accumulation rates and bedrock topography. In cold climatic conditions the frozen beds tend to be found in shallow ice with slow flow and low geothermal heat flux.

According to a hybrid ice-sheet/ice-stream model, approximately 20% of the Antarctic ice sheet is likely to be frozen to the bed, whereas the remainder is at the pressure-melting point[8]. Although the remote sensing observations provide estimates of ice thickness and bed elevation grids with rather high accuracy from few meters to the first tens of meters[9], the existence of subglacial water can only be detected if the water body is relatively thick (>1–2 m). These reservoirs are commonly referred to as subglacial lakes. By 2022, 675 subglacial lakes had been identified in Antarctica[10]. Cold- or warm-based settings between subglacial lakes are difficult or impossible to identify using remote sensing, and numerical models provide the basis for current understanding of the ice-bed interface conditions beneath the Antarctic ice sheet. However, different modeling approaches and uncertainties in the input data lead to a wide variety of warm-based/cold-based maps and estimates of the basal melting rates[11–13]. Only direct geological and geophysical field studies and observations in the boreholes drilled to the glacier bed can reliably disclose detailed information about the local thermodynamic state of the ice sheet.

[1]Institute of Polar Science and Engineering, College of Construction Engineering, Jilin University, Changchun, China. [2]School of Engineering and Technology, China University of Geosciences (Beijing), Beijing, China. [3]All-Russian Scientific Research Institute for Geology and Mineral Resources of the Ocean (VNIIO-keangeologia), St. Petersburg, Russia. [4]Institute of Earth Sciences, St. Petersburg State University, St. Petersburg, Russia. [5]Arctic and Antarctic Research Institute, St. Petersburg, Russia. [6]Key Laboratory of Polar Geology and Marine Mineral Resources, China University of Geosciences (Beijing), Beijing, China. [7]Institute of Geography, Russian Academy of Sciences, Moscow, Russia. [8]College of Geoexploration Science and Technology, Jilin University, Changchun, China.
✉e-mail: znan@jlu.edu.cn; bing@cugb.edu.cn

As in 2019, approximately 70,000 temperature and heat flow measurements have been made globally in the solid Earth surface[14], mostly in Europe, North America, and South Africa. At the same time, in Antarctica only a few dozen direct temperature measurements have been made in shallow bedrock boreholes in ice-free areas[15] and only three times so far in Antarctic subglacial till and bedrock[16–18]. That is almost nothing given that the total area of Antarctica covers approximately 14 million km², more than 10% of the Earth's land. The reason is obvious – drilling through thick ice is extremely complicated, time-consuming, and expensive. Alternative estimates of thermal conditions under the Antarctic ice sheet have been deduced from the steady-state heat flow modeling combined with estimates of vertical ice velocity and measured ice temperature profiles in boreholes that have succeeded in reaching or nearly reaching the ice sheet bed[19]. However, these data remain the only estimates.

Several multidisciplinary, international research programmes have been started recently, with the principal aims of improving the predictability of the thermo-hydrodynamic models for the Antarctic ice sheet and facilitating links between ice sheet modelers, geologists, solid-Earth geophysicists and glaciologists[20]. The carried out drilling project aimed at investigating the in-situ dynamics and conditions at the bed of the North-western Princess Elizabeth Land, East Antarctic Ice Sheet. The drill site selected for this mission is located approximately 28 km south of the coast of Prydz Bay (69.585591S; 76.385165E; 680 m asl) in the central part of the high-amplitude, linear magnetic anomaly crossing Princess Elizabeth Land and Mac. Robertson Land, above the top of the dome-shaped bedrock hill (Fig. 1)[21]. The nature of this anomaly remains unclear[22]. It may be related to the suture zone between ancient terrains formed during the Neoproterozoic amalgamation of the Rodinia supercontinent or to crustal accretion of the East Antarctic Craton in earlier times or to other tectonic events. The bedrock drilling is the only way to decipher the source of the magnetic anomaly and reconstruct the geodynamic history of the region through detailed studies of the sampled rocks.

The preliminary prognostic estimations (calculations are provided in the "Methods" section) performed before the drilling season, based on preliminary large-scale topographic data suggesting on average an ice sheet surface slope that is almost two times steeper, had pointed at a warm-based ice-bedrock interface with an overall melting rate of not less than 1–2 cm a^{-1} in the exploration area of radius 5-10 km. Our aim herein is to report on the direct geographical observations and temperature measurements at the base of the ice sheet at the chosen site and give updated detailed estimates of the basal temperature and melting rate distribution.

Results and discussion

The bedrock borehole was drilled between January and February 2024 (Fig. 2a). Critically, any access drilling activity must minimize all aspects of contamination of the subglacial environment in compliance with the Scientific Committee on Antarctic Research Code of Conduct[23]. Because preliminary estimations showed the warm-based conditions at the bed, it was decided to stop drilling ~10 m above the ice-bedrock interface, estimated as a result of a radar survey at a depth of 540–560 m, and to check for any evidence of refrozen water on the drill cutters.

On approaching the bed, the downhole control system of the drill indicated a low environmental temperature (<-5 °C) at the borehole bottom, and on February 24, 2024, the drill hit the bedrock at a depth of 541.12 m. The basal ice was solidly frozen to the bedrock and no visible signs of thawing were observed at this point.

Subsequently, a 0.48 m sample of bedrock core was recovered in two runs (Fig. 2b). The basal temperature of −4.52±0.2 °C was recorded at the bottom of the ice sheet 10 h after the drilling had been stopped, and appeared to be far below the pressure melting point (−0.35 °C) as it was expected. The real in-situ temperature may be even 0.5–1.0 °C lower due to thermal perturbations caused by drilling.

An important peculiarity of the borehole temperature distribution related to the downstream northward advection of colder ice masses along the flow line is the presen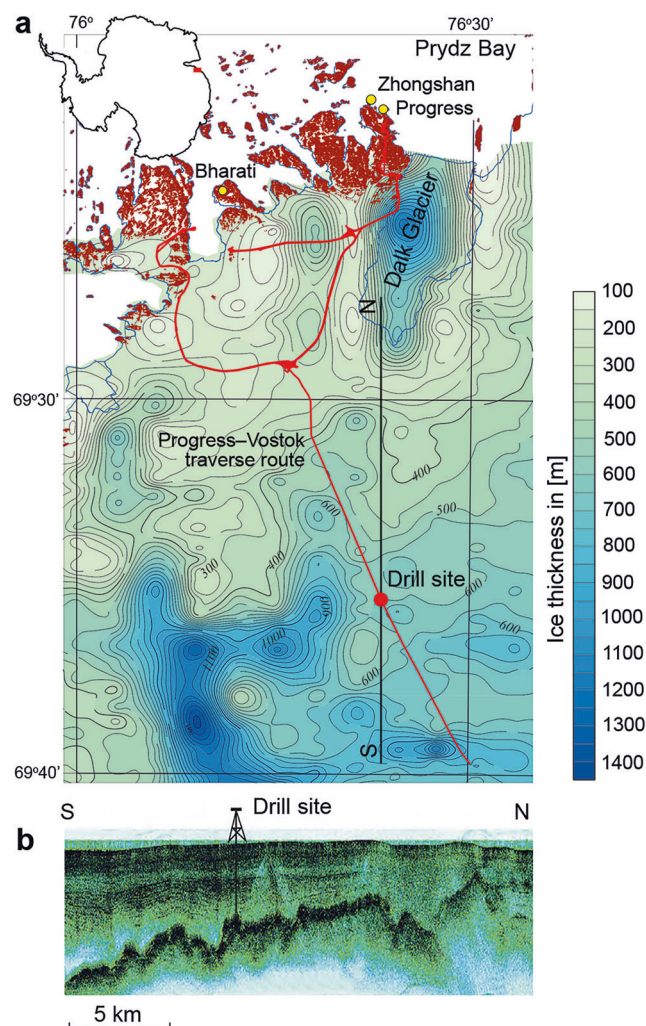ce of a negative temperature gradient in the upper part of the borehole (Fig. 3c). This occurs down to a depth of ~135 m with a measured temperature minimum of −18.12 °C. The temperature increase beneath this depth is generally controlled by the bedrock geothermal heat flux and internal strain heating in the underlying ice layers.

One could speculate that the single on-spot borehole temperature profile, which is influenced by various local topographic and geological factors, does not fully represent the mean regional geothermal background. Yet this difference between the preliminarily large-scale estimation and actually observed thermal regimes at the bed suggests that the Antarctic base could locally be much colder than currently assumed, and, as discussed below, thermo-hydrodynamic models, especially boundary conditions, should be carefully scaled to adequately describe the variable reality.

At the end of the field season, a radio-echo sounding survey was conducted around the drill site to clarify the surrounding thickness of the ice and bedrock topography[24]. The resulting maps show that the borehole is located very close to the bedrock hill summit, around which the ice thickness increases from 541 m at the drilling site to ~575 m in the nearest vicinities of 200 m and up to ~670 m upstream, 1-2 km southward. The elevation of the bedrock under the drill site is 132 m asl and it increases slightly towards the northeast up to 136 m asl. This indicates that the ice-sheet surface slope along the flow line, being ~0.01-0.02 at the drilling site, grows up to ~0.03 on average outside the subglacial hill.

Fig. 1 | Location of the drill site. a Area of study in the northwestern Princess Elizabeth Land, East Antarctic Ice Sheet with ice thickness isolines; the red line shows the location of the traverse route between the coast and the inland Vostok Station. **b** Radio-echo sounding profile across the drill site (the horizontal scale of the profile is the same as the scale of the map).

Fig. 2 | Drilling to the bed at the northwestern Princess Elizabeth Land, East Antarctic Ice Sheet. a Bird's eye view of the drilling camp showing the drilling shelter, workshop, living shelters, and auxiliary facilities in northwestern Princess Elizabeth Land, East Antarctica. **b** The upper (18 cm long) part of the subglacial bedrock core from a depth of 541.12-541.30 m is presented by metamorphic rock of dolerite composition.
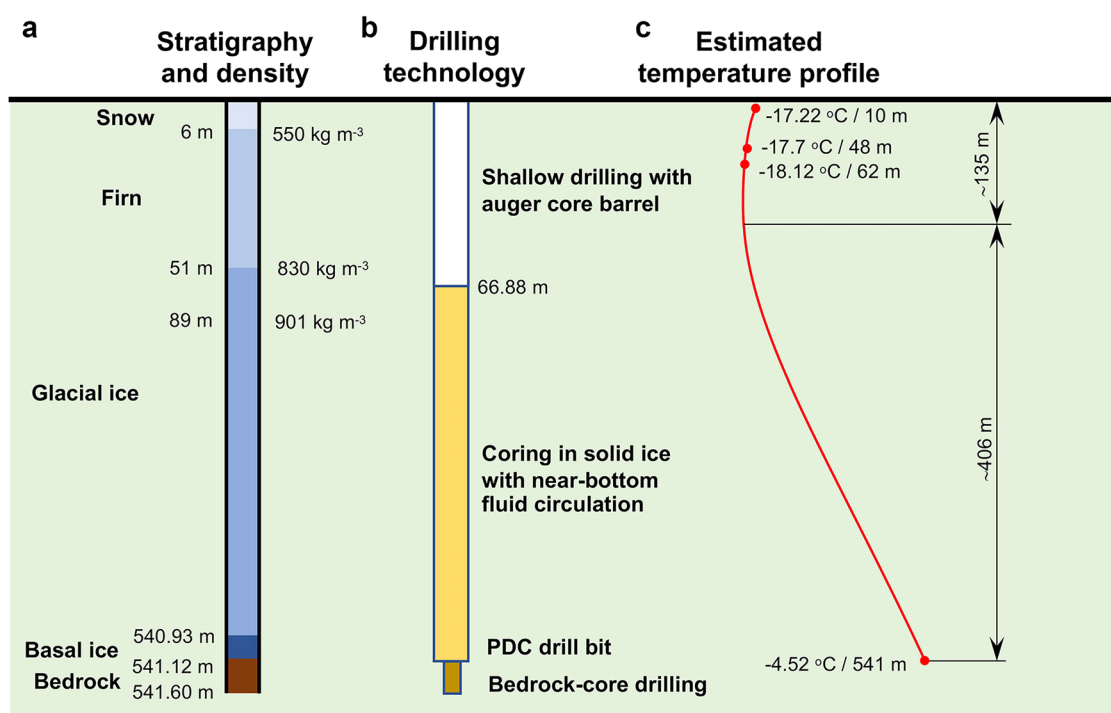

Fig. 3 | Schematic of core stratigraphy, drilling technology sequence and estimated temperature profile (not to scale). a The stratigraphy is typical for the dry-snow accumulation zone. The boundaries between snow, firn, and bubbly ice are defined by core density[47] and are conventionally drawn at densities of about 550 kg m⁻³ and 830 kg m⁻³. **b** The borehole construction consisted of the following steps: (1) dry core drilling of the upper permeable snow–firn layer with an auger drill; (2) fluid core drilling of glacial ice using bottom fluid reverse circulation; (3) drilling through debris-rich ice with a PDC drill bit; and (4) bedrock core drilling. **c** The measured borehole temperature (red dots) and estimated temperature profile with a zone with a negative geothermal gradient down to a depth of ~135 m. Further down, the temperature profile increases with depth with an approximate mean gradient of 3.5 °C / 100 m.

The data obtained during the drilling season allow us to carry out much deeper quantitative analysis of the local thermal state of the ice sheet. Our refined thermal modeling estimates show that the internal strain heating increases from 90 mW m⁻² at the drill site to 330 mW m⁻² 1-2 km south of it. The temperature increase below the minimum temperature level through the 406 m ice layer with a positive downward temperature gradient at the drilling site can be estimated at Glen's flow law exponent $\beta = 1$ and $\beta = 6$ within the respective ranges of 12.3-13.6 °C and 13.6-14.9 °C for the minimum surface slope of 0.01 and geothermal flux of 45-55 mW m⁻². The temperature growth does not exceed 20.8-23.3 °C in the limiting case of maximum slope 0.02 and heat flux 55 mW m⁻² for $\beta = 1$-6. The deduced

estimates are closely consistent with the observed temperature increase value of 14.5 °C. As mentioned above, the minimum in-situ ice temperature at the drilling site was measured at −18.12 °C, also confirming the available heat-flux estimates and their agreement with the cold-based glacier observations.

Nevertheless, one could further speculate on predicting the thermal conditions on the bedrock several kilometers away from the drilling site where the ice sheet thickness increases to ~ 670 m, and surface slope rises to ~ 0.03, while the positive downward temperature gradient covers the lower ~507 m. The results of the calculations would show a twofold increase in temperature (~34-39 °C on average) below the depth of the minimum temperature, thus indicating an excessive overheating of 15-25 °C in the
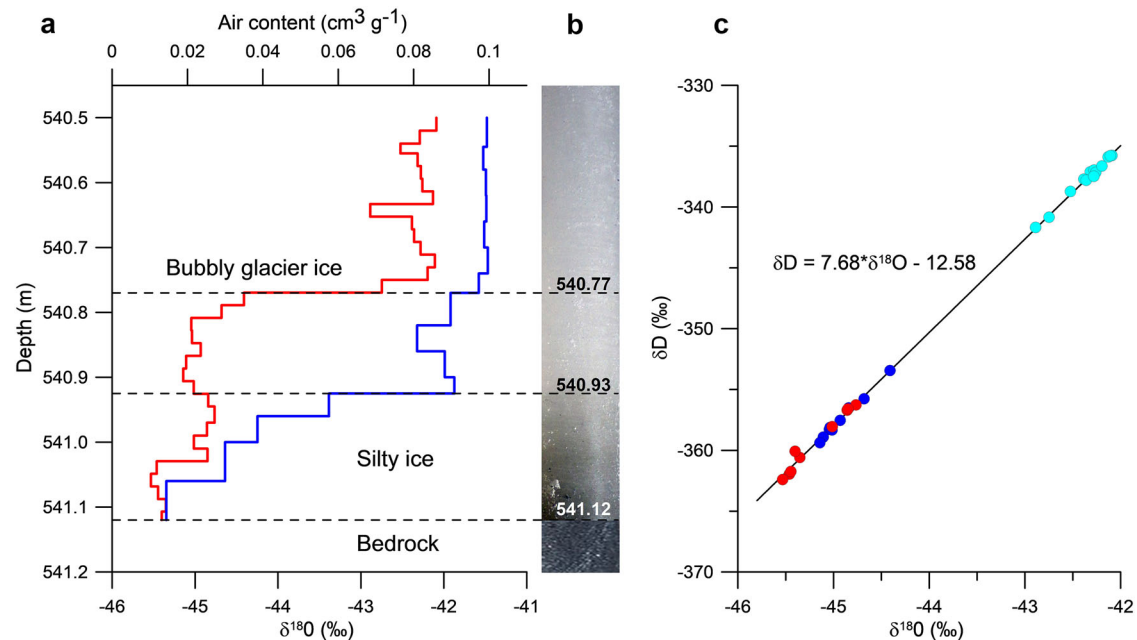
Fig. 4 | Isotope composition and air content of the bottom part of the ice core. a Air content (blue) and $\delta^{18}O$ (red) vs. depth. **b** The visual appearance of the ice core. **c** The δD–$\delta^{18}O$ values obtained in layers 540.50−540.77 m (cyan), 540.77-540.93 m (blue), and 540.93-541.12 m (red) are located on the local meteoric water line.

absence of basal melt. This means that the warm-based vicinities likely surround the drilling site with the basal melting rate on the order of ~1-2 cm a^{-1} to compensate the internal or basal strain heating.

In order to investigate whether the bottom ice at the drilling site had been previously subjected to melting and re-freezing, we studied the isotopic composition (δD and $\delta^{18}O$) and total air content of the bottommost 62 cm piece of drilled ice core, the only one so far delivered from Antarctica to the laboratory. The results seem to support a warmer bed upstream of the drilling site. The upper part of the studied core, between 540.50 and 540.77 m, comprises bubbly glacier ice, apparently not much affected by the near-bed processes. The mean values of isotopic composition ($\delta^{18}O$ = -42.3 ‰) and air content (0.099 $cm^3 g^{-1}$) in this depth interval are significantly lower than the present-day values expected at the drilling site, about -20 ‰[25] and 0.125 $cm^3 g^{-1}$ [26], respectively (Fig. 4a). According to the present-day spatial distribution of $\delta^{18}O$ and air content of ice in Antarctica versus elevation[25–27], ice with such properties could have formed upstream of the drilling site, at an elevation of about 2600 m.

At a depth of 540.77 m there is a sharp decrease in the heavy isotope and air content of ice. In the layer bedded between 540.77 and 540.93 m the mean isotope composition (-44.9 ‰) and the air content of ice (0.087 $cm^3 g^{-1}$) are typical of Holocene ice that formed farther inland at an elevation of about 2900-3100 m or, alternatively, are evidence of ice formed in a colder climate. Final conclusions on this can be drawn only after studies of the entire 540 m ice core have been completed.

Finally, from 540.93 m to the contact with the rocky bed at 541.12 m, a layer of silty ice containing bedrock particles is observed (Fig. 4b). The amount of air in this layer decreases with increasing depth and reaches a level well below that characteristic of polar ice, clearly indicating that at least part of this ice has undergone melting and subsequent refreezing. Interestingly, the presence of refrozen water had no effect on the isotope content of the silty ice. Indeed, the δD–$\delta^{18}O$ diagram (Fig. 4c) shows that all data points are located on the same straight line with a slope of about 7.7, which is typical for Antarctic precipitation[27], whereas in the case of ice formed from water frozen in a closed system, a smaller slope should be expected[22]. Thin-section studies of silty ice showed that it is an aggregate of bubbly glacier ice and lenses of refrozen water containing rare microbubbles. The lenses are about 1 cm thick, which is half the thickness of our isotopic samples. It is for this reason that isotopic changes in these lenses could not be detected, and

our measurements could only give their average isotopic composition, which is equal to that of meltwater and of the original ice that melted[28].

The step change in heavy isotope and air content at 540.77 m (Fig. 4a) and the gap in the data points in the δD–$\delta^{18}O$ diagram (Fig. 4c) suggest a discontinuity of the ice column at this depth. We hypothesize that the core below 540.77 m represents a sample of older ice residing upstream of the drilling site, where the basal melting prevails due to the enhanced strain heating, and from where a small upper portion of this ice has been grabbed by the glacier and dragged, along with trapped bedrock particles, to the top of the subglacial hill.

In this analysis, we present the first results of the drilling project which succeeded in penetrating 541 m thick ice at the northwestern margin of Princess Elizabeth Land. 0.48 m of high-quality bedrock core has been recovered. Our study of the basal thermal regime in this borehole found a fundamental difference between the preliminarily modeled and real thermal conditions at the bed of the ice sheet. This gives weight to the idea that local geological, topographic and flow setting are critical for understanding the behavior of alternating warm- and cold-based areas of the Antarctic bed. In turn, local deviations can lead to serious errors in large-scale projection of the Antarctic basal thermal regime and ice-sheet mass loss. Because of the high natural variability of the basal conditions, we ultimately want a number of such boreholes in order to verify thermal models and sea-level rise projections. Now, this may appear to be a distant dream; however, subglacial drilling in Antarctica will only become more routine and cheaper with time and experience.

Methods
Drilling
All the drilling equipment was installed inside a movable, sledge-mounted, temperature-controlled, and wind-protected drilling shelter[29]. The drilling technology utilizes an electromechanical cable-suspended drill designed for drilling in firn, ice, debris-rich ice, and rock[30]. The changeable modules of the drill allow different tasks to be carried out (Fig. 3b). The upper snow–firn layers to a depth of 66.88 m were drilled with an auger-core barrel. In total, 101 runs were performed to penetrate the snow-firn layers. The firn density reached 830 kg m^{-3} at a depth of 51 m. At this stage, a run took 25–30 min on average, and the mean core length was about 0.66 m. When impermeable glacial ice was reached, the borehole was filled with drilling fluid (kerosene-

type fuel, Jet A1) to a height of approximately 10 m above the bottom. Drilling was continued with another version of the drill designed for coring with fluid circulation. The lower part of the drill comprised a single core barrel with sharp cutters and a filter chip chamber. The inner/outer diameters of the ice-core drill head were 105/136 mm. The average daily production was 18–24 m day^{-1} with the core yield of about 1.1 m per run. At the approach to the bed, a PDC drill bit was installed for drilling debris-containing ice. The final stage included drilling the bedrock with a toothed diamond bit and a 1 m long conventional single-core barrel, a chip chamber for gravity separation of rock cuttings, and adjustable deadweights to increase the load on the diamond bit. The inner/outer diameters of the diamond bit were 41/60 mm. A total of 48 cm of bedrock samples were recovered in two runs.

In order to avoid the potential for biological and chemical contamination of the subglacial environment by drilling fluid and subsequent impact on microbial function, it was decided to stop drilling ∼10 m above the ice-bedrock interface. However, it was found that the drilling site is located in a cold-based area with a frozen bed, which excludes the ingress of drilling fluid into subglacial water. In the 2024–2025 season, it is planned to recover drilling fluid from the borehole using downhole bailer[31]. In total, 32 L of drilling fluid is collected in one bailing run with a 3 m-long bailer. It is assumed that the volume of the fluid left in the borehole will not exceed 10 L. To remove drilling fluid from the borehole, it will be necessary to carry out about 240 bailing runs. With round-the-clock operation, this would take 4–5 days.

Temperature measurements

The onboard drill's Pt100 temperature sensor, of the CWDZ11-Z-05 type (with accuracy of ± 0.1 °C), allowed real-time temperature control in the borehole[32]. However, these measurements were inevitably affected by the drilling process and did not directly represent the original ice temperature. With this in mind, four point-by-point measurements were additionally carried out by a K-type thermocouple temperature sensor with accuracy of ±0.2 °C (Fig. 3c). During this temperature survey, the drill was removed from the borehole and the sensor was delivered to the target depth, using specialized thin steel cable with depth marks, coiled on a small hand winch. At each of the four depth levels, the thermal equilibration of the sensor in the borehole took about 24 h. The collected temperature data from the sensor were stored in its internal memory. When the logging procedure at a certain depth was finished, the sensor was lifted back to the surface, and all stored temperature measurements were retrieved via computer connection. When analyzing each data set, only the latest stabilized readings were selected as representative accurate steady-state temperatures corresponding to that specific depth.

Ground-penetrating radar profiling

The survey was carried out using a VIRL-7 radio-echo sounding system with a central frequency of 20 MHz[33]. The radar components (receiver, transmitter, registration unit, power supplies, antennas and GPS) were placed on two sledges and moved by one operator along several profiles around the drill site at a distance of 25–200 m. In total, 2.5 km radar profiles were obtained. To convert the delay time of the signals into thickness values, the average propagation velocity of electromagnetic waves was taken as 174 m/μs.

Thermal modeling at the ice sheet base

Below melting point, without bottom sliding, the internal strain heating density q(h) is non-linearly distributed in the glacier body versus the ice-equivalent distance h from the bottom[34]

$$q = g\rho_0 \left|\frac{\partial l}{\partial s}\right| U_0(\beta + 1)(1 - \zeta)^{\beta+1}, \quad \zeta = \frac{h}{\Delta_0} \tag{1}$$

Here g is the gravity acceleration; ρ_0 is the average ice density (920 kg m^{-3}); Δ_0 is the glacier thickness in the ice equivalent; $\partial l/\partial s$ is the surface slope; U_0 is

the ice-surface velocity at the drill site determined on the basis of two months of GPS observations as ∼60 m a^{-1}; β is the typically large modified Glen's flow law exponent (β ∼ 6)[34,35].

Accordingly, the cumulative strain heating below h-level is

$$Q(h) = Q_0 \frac{\beta + 1}{\beta + 2} \left[1 - (1 - \zeta)^{\beta+2}\right], \quad Q_0 = g\rho_0 \Delta_0 \left|\frac{\partial l}{\partial s}\right| U_0 \tag{2}$$

where Q_0 can be interpreted as basal strain heating concentrated at the bed proximity in the limiting case of β → ∞. It is easy to see that Q(h) remains practically constant, except for the basal layer ζ < 1/(β + 2), increasing on average the geothermal heat flux q_0 (GHF) by additional apparent heat flow

$$\overline{Q}_0 = Q_0 \frac{\beta + 1}{\beta + 3} \tag{3}$$

As a result, in one-dimensional quasi-steady approximation below the upper zone of negative temperature anomaly the heat transfer equation[34] reduces to the following simplified form:

$$Pe\zeta \frac{\partial T}{\partial \zeta} + \frac{\partial^2 T}{\partial \zeta^2} = 0 \tag{4}$$

which at the given basal heat flux $q_0 + \overline{Q}_0$ directly leads to the temperature gradient

$$\frac{\partial T}{\partial h} = -\frac{q_0 + \overline{Q}_0}{\lambda} \exp\left(-\frac{Pe}{2}\zeta^2\right) \tag{5}$$

Here the dimensionless Peclet number, $Pe = \rho_0 cb\Delta_0/\lambda$, is expressed via the average thermal conductivity[36] λ = 2.35 W (m °C)$^{-1}$ and specific heat capacity[34] c = 2.04 kJ (kg °C)$^{-1}$ of ice at −10 °C, and via the local ice accumulation rate b ≈ 0.35 m a^{-1} in ice equivalent.

The snow-firn accumulation/densification regime at the drilling location (Fig. 3a) is closely comparable to that of the H-72 site (East Antarctica)[37]. As a consequence, the ice-equivalent thickness Δ_0 is about 20 m less, that is, 521 m at the drill site, growing presumably to ∼650 m at a 1-2 km distance southward upstream from the borehole, with respective Peclet values being on the order of Pe ∼ 4-5. It is assumed that the ice thickness below h_0 -level of the temperature minimum increases proportionally (by 25%) from ∼406 m at the drill site (Fig. 3a) to ∼507 m outside the subglacial hill. Further on, one can predict that the derived estimate of the temperature gradient in the glacier body is approximately applicable below this level for ζ < 0.78 and $0.5Pe\zeta^2$ < 1.2–1.5. Under these conditions the integration of the above ∂T/∂h-expression with the use of the error function erf(x) results in the following temperature drop across the h_0-layer:

$$\Delta T = \frac{\Delta_0}{\lambda}\left(q_0 + Q_0 \frac{\beta + 1}{\beta + 3}\right)\sqrt{\frac{\pi}{2Pe}} erf\left(\frac{h_0}{\Delta_0}\sqrt{\frac{Pe}{2}}\right)$$

$$\approx (0.69 \pm 0.02)\frac{h_0}{\lambda}\left(q_0 + Q_0 \frac{\beta + 1}{\beta + 3}\right) \tag{6}$$

Obviously q_0 here is another principal characteristic that controls the thermal (warm-/cold-based) state of the glacier. The regional GHF averages estimated for this area based, generally, on a tectonic setting vary[38–41] from 55 to 65 mW m^{-2}. These bounds also cover possible local refraction effects[42] that might be induced by undulations of the bedrock relief at diorite thermal conductivity higher than that of ice. The relatively low thermal conductivity of ice globally reduces on average the background level of the GHF under the thick ice sheet to lower values. Thus, the GHF at the drill site can be taken[14,34,43,44] presumably in the range of 45–55 mW m^{-2}.

Isotope and gas core analyses

For stable water isotope measurements of the lowest 62 cm of the ice core we used the Picarro L2140-i laser analyzer. The 32 samples were cut continuously with a 2 cm resolution from the 540.50–541.12 m core interval. Each sample was measured twice using two different laboratory standards (VOS-4 and VSPB-2 with the δD values equal to -439.7 and -207.0 ‰, and $\delta^{18}O$ values equal to -56.81 and -26.70‰, respectively), calibrated to IAEA's standards VSMOW-2, SLAP-2 and GISP. The standards were measured after every 5 measurements of samples in order to calculate the true isotopic values of samples based on their measured values. The reproducibility of the measurements was 0.53‰ for δD and 0.05‰ for $\delta^{18}O$.

The air content measurements were carried out using an original barometrical method implemented with an experimental setup called STAN[45]. The STAN allows precise evaluation of the pressure and temperature of air extracted from an ice sample by its melting and refreezing under a vacuum in a volume-calibrated cell. After correcting the measured pressure for the partial pressure of saturated water vapor and of the calibrated volume for the volume occupied by refrozen bubble-free ice, the air content (traditionally expressed in cm^3 (STP) of dry air per 1 g of ice) is calculated using the ideal gas law. The ice samples used for measurements had a mass of 15–25 g and the shape of a rectangular prism, which facilitated estimation of their specific surface area. The latter is needed to correct data for the gas loss from air inclusions cut at the surface of the sample. The correction depends on the specific surface of the ice sample and the sizes of the air inclusions[46]. The sizes of the air inclusions were measured under a binocular microscope in 2–4 mm thick sections of ice cut in parallel with the samples used for air content measurements. The absolute precision of the STAN measurements has been estimated to be within ±0.6%. However, the overall error of the obtained air content values amounts to 1% due to uncertainties in the cut-bubble correction[45].

Data availability

Drilling records and data related to studies of the isotopic composition and the total air content in the basal ice are available for download from http://cerl-aari.ru/index.php/anomaly/.

References

1. Fox-Kemper, B. et al. Ocean, Cryosphere and Sea Level Change. In Climate Change 2021: The Physical Science Basis. *Contribution of Working Group I to the Sixth Assessment Report of the Intergovernmental Panel on Climate Change*. Cambridge University Press, Cambridge, United Kingdom and New York, NY, USA, pp. 1211–1362 (2021).
2. Dawson, E. J. et al. Ice mass loss sensitivity to the Antarctic ice sheet basal thermal state. *Nat. Commun.* **13**, 4957 (2022).
3. Park, J. Y. et al. Future sea-level projections with a coupled atmosphere-ocean-ice-sheet model. *Nat. Commun.* **14**, 636 (2023).
4. Siahaan, A. et al. The Antarctic contribution to 21st-century sea-level rise predicted by the UK Earth System Model with an interactive ice sheet. *The Cryosphere* **16**, 4053–4086 (2022).
5. Aitken, A. R. A. Antarctic sedimentary basins and their influence on ice-sheet dynamics. *Rev. Geophys.* **61**, e2021RG000767 (2023).
6. Van Liefferinge, B. et al. Promising Oldest Ice sites in East Antarctica based on thermodynamical modelling. *The Cryosphere* **12**, 2773–2787 (2018).
7. Sun, B. et al. How old is the ice beneath Dome A, Antarctica? *The Cryosphere* **8**, 1121–1128 (2014).
8. Pattyn, F. Antarctic subglacial conditions inferred from a hybrid ice sheet/ice stream model. *Earth Planet. Sc. Lett.* **295**, 451–461 (2010).
9. Frémand, A. C. et al. Antarctic Bedmap data: Findable, Accessible, Interoperable, and Reusable (FAIR) sharing of 60 years of ice bed, surface, and thickness data. *Earth Syst. Sci. Data* **15**, 2695–2710 (2023).
10. Livingstone, S. J. et al. Subglacial lakes and their changing role in a warming climate. *Nat. Rev. Earth Environ.* **3**, 106–124 (2022).
11. Huang, Y. et al. Using specularity content to evaluate eight geothermal heat flow maps of Totten Glacier. *The Cryosphere* **18**, 103–119 (2024).
12. Park, I.-W. et al. Impact of boundary conditions on the modeled thermal regime of the Antarctic ice sheet. *The Cryosphere* **18**, 1139–1155 (2024).
13. Dawson, E. J. et al. Heterogeneous basal thermal conditions underpinning the Adélie-George V Coast, East Antarctica. *Geophys. Res. Lett.* **51**, e2023GL105450 (2024).
14. Lucazeau, F. Analysis and mapping of an updated terrestrial heat flow data set. *Geochem. Geophys. Geosys.* **20**, 4001–4024 (2019).
15. Burton-Johnson, A., Dziadek, R. & Martin, C. Review article: geothermal heat flow in Antarctica: current and future directions. *The Cryosphere* **14**, 3843–3873 (2020).
16. Zotikov, I. A Izmerenie geotermicheskogo potoka tepla v Antarktide [Measurement of the geothermal heat flow in Antarctica]. 29, 30–32 (1961).
17. Fisher, A. T. et al. High geothermal heat flux measured below the West Antarctic Ice Sheet. *Sci. Adv.* **1**, e1500093 (2015).
18. Begeman, C. B. et al. Spatially variable geothermal heat flux in West Antarctica: Evidence and implications. *Geophys. Res. Lett.* **44**, 9823–9832 (2017).
19. Talalay, P. et al. Geothermal heat flux from measured temperature profiles in deep ice boreholes in Antarctica. *The Cryosphere* **14**, 4021–4037 (2020).
20. Colleoni, F. et al. The uncertain future of Antarctica's melting ice. *Eos* **103** https://doi.org/10.1029/2022EO220014 (2022).
21. Golynsky, A. V. et al. The composite magnetic anomaly map of the East Antarctic. *Tectonophysics* **347**, 109–120 (2002).
22. Leitchenkov G. L. et al. First targeted geological sampling beneath the East Antarctic Ice Sheet: Joint Russian-Chinese drilling project. *Exploration & Protection of Mineral Resources* **Spec**. **Issue July**, 75–78 (2024).
23. Siegert, M. J. & Kennicutt, M. C. Governance of the exploration of subglacial Antarctica. *Front. Environ. Sci.* **6**, 1–6 (2018).
24. Leitchenkov, G. L. et al. Burenie l'da na Zemle Princessy Elizavety (Vostochnaya Antarktida) dlya izucheniya geologii korennogo lozha i pozdnechetvertichnogo klimata [Ice drilling on Princess Elizabeth Land (East Antarctica) aimed to study bedrock and Late Quaternary paleoclimate. **64**, 293–298 (2024).
25. Pang, H. et al. Spatial distribution of 17O-excess in surface snow along a traverse from Zhongshan station to Dome A, East Antarctica. *Earth Planet. Sci. Lett.* **414**, 126–133 (2015).
26. Martinerie, P. et al. Physical and climatic parameters which influence the air content in polar ice. *Earth Planet. Sci. Lett.* **112**, 1–13 (1992).
27. Masson-Delmotte, V. et al. A review of Antarctic surface snow isotopic composition: Observations, atmospheric circulation, and isotopic modeling. *J. Clim.* **21**, 3359–3387 (2008).
28. Jouzel, J. & Souchez, R. A. Melting-refreezing at the glacier sole and the glaciological composition of the ice. *J. Glaciol.* **28**, 35–42 (1982).
29. Talalay, P. et al. Antarctic subglacial drilling rig: Part I. General concept and drilling shelter structure. *Ann. Glaciol.* **62**, 1–11 (2021).
30. Talalay, P. et al. Antarctic subglacial drill rig. Part II: Ice and Bedrock Electromechanical Drill (IBED). *Ann. Glaciol.* **62**, 12–22 (2021).
31. Fan, X. et al. Antarctic subglacial drilling rig: Part III. Drilling auxiliaries and environmental measures. *Ann. Glaciol.* **62**, 24–33 (2021).
32. Zhang, N. et al. Antarctic subglacial drilling rig: Part IV. Electrical and electronic control system. *Ann. Glaciol.* **62**, 34–45 (2021).
33. Vasilenko, E. V. et al. A compact lightweight multipurpose ground-penetrating radar for glaciological applications. *J. Glaciol.* **57**, 1113–1118 (2011).
34. Salamatin, A. N. et al. Ice flow line modeling and ice core data interpretation: Vostok Station (East Antarctica), Physics of Ice Core

Records-II. In *Low Temperature Science* (T. Hondoh, Ed.), Supplement Issue ILTS, **68**, pp. 167–194 (Hokkaido University, Sapporo, 2009).

35. Lliboutry, L. A critical review of analytical approximate solutions for steady state velocities and temperatures in cold ice sheets. *Z. Gletscherkd. Glazealgeol* **15**, 135–148 (1979).

36. Slack, G. A. Thermal conductivity of ice. *Phys. Rev. B* **22**, 3065–3071 (1980).

37. Salamatin, A. N. et al. Snow-firn densification in polar ice sheets, Physics of Ice Core Records-II. In *Low Temperature Science* (T. Hondoh, Ed.), Supplement Issue ILTS, **68**, pp. 195–222 (Hokkaido University, Sapporo, 2009).

38. An, M. et al. Temperature, lithosphere-asthenosphere boundary, and heat flux beneath the Antarctic Plate inferred from seismic velocities. *J. Geophys. Res. Solid Earth* **120**, 8720–8742 (2015).

39. Martos, Y. M. et al. Heat flux distribution of Antarctica unveiled. *Geophys. Res. Lett.* **44**, 11417–11426 (2017).

40. Lösing, M. & Ebbing, J. Predicting geothermal heat flow in Antarctica with a machine learning approach. *Geophys. Res. Solid Earth* **126**, e2020JB021499 (2021).

41. Stål, T. et al. Antarctic geothermal heat flow model: Aq1. *Geochem. Geophys. Geosyst.* **22**, e2020GC009428 (2021).

42. Willcocks, S. et al. Thermal refraction: implications for subglacial heat flux. *J. Glaciol.* **67**, 875–884 (2021).

43. Siegert, M. J. & Dowdeswell, J. A. Spatial variations in heat at the base of the Antarctic ice sheet from analysis of the thermal regime above subglacial lakes. *J. Glaciol.* **42**, 501–509 (1996).

44. Siegert, M. J. et al. Physical, chemical and biological processes in Lake Vostok and other Antarctic subglacial lakes. *Nature* **414**, 603–609 (2001).

45. Lipenkov, V. et al. A new device for the measurement of air content in polar ice. *J. Glaciol.* **41**, 423–429 (1995).

46. Martinerie, P. et al. Correction of air-content measurements in polar ice for the effect of cut bubbles at the surface of the sample. *J. Glaciol.* **36**, 299–303 (1990).

47. Anderson, D. L. & Benson G. S. The densification and diagenesis of snow: properties, processes and applications. In Kingery, V. V. D., ed. Ice and snow: properties, processes, and applications. Cambridge, MA, M.I.T. Press, pp. 391–411 (1963).

Acknowledgements

Author contributions

P.G.T., G.L., V.L., A.S., and A.A.E. developed the concept and wrote the manuscript. Yo.S., N.Z., X.F., and B.L. contributed to the design and implementation of the research. A.S. provided borehole thermal regime estimations. V.L. and A.A.E. carried out ice core studies and interpretations of the basal ice. D.G., Y.Liu, Y.Li, Yu.S., I.A., M.V., and D.K. took part in the field operations and carried out borehole temperature measurements.

Competing interests

The authors declare no competing interests.

Additional information